Lattice instabilities of cubic NiTi from first principles

Xiangyang Huang, Claudia Bungaro, Vitaliy Godlevsky, and Karin M. Rabe
Department of Physics and Astronomy, Rutgers University, Piscataway, New Jersey 08854-8019
(Received 15 May 2001; revised manuscript received 24 August 2001; published 6 December 2001)

The phonon dispersion relation of NiTi in the simple cubic $B2$ structure is computed using first-principles density-functional perturbation theory with pseudopotentials and a plane-wave basis set. The structure is shown not to be a local energy minimum, so that its observation at high temperatures must be due to entropic stabilization by large fluctuations around the average atomic positions. Lattice instabilities are observed to occur across nearly the entire Brillouin zone, excluding three interpenetrating tubes of stability along the (001) directions and small spheres of stability centered at R. The strongest instability is that of the doubly degenerate $M_{5'}$ mode. The distorted structure produced by freezing a particular choice of unstable $M_{5'}$ eigenvector into the reference cubic structure yields, with an appropriate choice of overall amplitude, an excellent approximation to the observed ground-state $B19'$ structure.

DOI: 10.1103/PhysRevB.65.014108 PACS number(s): 63.20.−e, 64.60.−i

I. INTRODUCTION

The realization of the technological promise of active materials requires significant progress in the fundamental understanding of their nature and behavior. Similarities between different classes of active materials, such as piezoelectric oxides and shape memory alloys, suggest that theoretical analysis successful for one class might also be productively applied to another. For example, first-principles calculations of the type previously applied to structural transitions in the perovskite oxides[1–4] should also yield insight into the properties of shape memory alloys.

The relative chemical and structural simplicity of the shape memory alloy NiTi has made it a popular subject of both experimental and theoretical study.[5] At high temperatures, NiTi is observed to have the cubic $B2$ structure. The structural phase transition at 333 K suggests that the $B2$ structure is not a local energy minimum, but rather is entropically stabilized by fluctuations around the average atomic positions, similar to the high-temperature cubic perovskite phases of $BaTiO_3$ and $PbTiO_3$. The monoclinic $B19'$ low-temperature structure of NiTi is related to the $B2$ structure by approximately rigid shifts of alternate (110) planes along the $(1\bar{1}0)$ direction, resulting in a lowering of the symmetry and a corresponding change in the shape of the unit cell.[6] Previous first-principles studies have focused on accurate prediction of the ground-state structural parameters by relaxing forces and stresses for a particular choice of space group, complementing the experimental structural determination data.[7,8]

The distortion that relates the two structures has the symmetry of a single M-point normal mode of the $B2$ structure. There is thus a parallel between the martensitic transformation from the $B2$ to the $B19'$ structure in NiTi and the paraelectric-ferroelectric ''soft-mode'' transition in perovskite oxides such as $PbTiO_3$, $BaTiO_3$, and $KNbO_3$,[9] for which the distortion that relates the high-temperature and low-temperature structures has the symmetry of a single normal mode of the cubic perovskite structure (at Γ). In these perovskites, first-principles calculation of the eigenfrequencies and eigenvectors of the unstable phonons of the cubic high-symmetry prototype structure[2–4] has shown that an excellent approximation to the ferroelectric ground-state structure is obtained by ''freezing in'' the single dominant unstable phonon (a polar optic mode at the zone center) with an accompanying change in the shape of the unit cell. The $\vec{q}$ dependence of the instability across the Brillouin zone has been shown to determine the nature of the local structural fluctuations that entropically stabilize the high-temperature cubic paraelectric phase[2] and, through a first-principles effective Hamiltonian analysis, to determine the transition temperature and related quantities as well.[4]

In this paper, we take the first step in extending this approach to shape memory alloys by computing the phonon eigenfrequencies and eigenvectors of the cubic high-symmetry prototype structure of NiTi from first principles, as described in Sec. II. In Sec. III, the dominant unstable phonon is identified and the structure it generates is compared with available knowledge of the ground state structure. We then examine how these instabilities extend across the Brillouin zone, analyzing the dispersion to obtain values for real-space interatomic force constants and identifying the minimal unstable localized atomic displacement pattern. We conclude by speculating on the implications of these results on the structure and properties of the high-temperature phase and on the martensitic transition.

II. COMPUTATIONAL METHOD

First-principles calculations of the structural energetics of $B2$ NiTi were carried out within density-functional theory with a plane-wave pseudopotential approach. Phonon eigenfrequencies and eigenvectors throughout the Brillouin zone were obtained using the Green's function formulation of density-functional perturbation theory (DFPT).[10] The calculations were performed with the PWSCF and PHONON codes,[11] using the Perdew-Zunger[12] parametrization of the local-density approximation (LDA). For comparison, dynamical matrices at selected $\vec{q}$-points were also computed with the generalized gradient approximation (GGA).[13] Ultrasoft pseudopotentials[14] for Ti and Ni were generated according to

TABLE I. Lattice parameter and elastic constants of NiTi in the $B2$ structure. The FLAPW of a_0 in the parentheses is computed with GGA.

	PW	MB (Ref. 7)	FLAPW	Exp.
a_0(a.u.)	5.594	5.626	5.561(5.670)	5.698 (Ref. 20)
B (Mbar)	1.68	1.56	1.86	1.40 (Ref. 21)
c_{11} (dyn/cm^2)	1.80	1.68	-	1.62 (Ref. 21)
c_{12} (dyn/cm^2)	1.62	1.44	-	1.29 (Ref. 21)
c_{44} (dyn/cm^2)	0.39	0.50	-	0.35 (Ref. 21)

a modified Rappe-Rabe-Kaxiras-Joannopoulos (RRKJ) scheme[15] with three Bessel functions.[16] The electronic wave functions were represented in a plane-wave basis set with a kinetic energy cutoff of 30 Ry. The augmentation charges were expanded up to 660 Ry. The Brillouin zone (BZ) integrations were carried out by the Hermite-Gaussian smearing technique[17] using a 56 k-point mesh (corresponding to $12\times12\times12$ regular divisions along the k_x, k_y, and k_z axes) in the $\frac{1}{48}$ irreducible wedge. The value of the smearing parameter was $\sigma=0.02$ Ry. These parameters yield phonon frequencies converged within 5 cm^{-1}. The dynamical matrix was computed on a $6\times6\times6$ $\vec{q}$-point mesh commensurate with the k-point mesh. The complete phonon dispersion relation was obtained through the computation of real-space interatomic force constants within the corresponding box.[18]

In Table I, we report the equilibrium lattice parameter and elastic constants of $B2$ NiTi obtained from pseudopotential total energy calculations performed as described above, and from a previous pseudopotential calculation using a mixed basis (MB) set.[7] For comparison, we also performed full-potential linearized-augmented-plane-wave calculations (FLAPW) within both the LDA and GGA.[19] The lattice parameter and bulk moduli were obtained from a Birch function fit.[22] The discrepancy between the PWSCF and FLAPW values for the LDA lattice parameter is comparable ($<1\%$) to that between the two pseudopotential results. The FLAPW lattice parameter is slightly larger within GGA, as expected, and the bulk moduli show the typical decrease with increasing lattice parameter. Although these results are not directly comparable with the properties of the entropically stabilized high-temperature $B2$ phase, characterized by large fluctuating atomic displacements, the experimental data included in Table I are in general agreement with the first-principles values. The DFPT calculations reported in the next section were performed at the PWSCF lattice parameter 5.594 a.u.

III. RESULTS AND DISCUSSION

The full phonon dispersion of $B2$ NiTi consists of six branches: three acoustic and three optic. Results of our calculations along the high-symmetry lines of the simple cubic BZ are shown in Fig. 1. The imaginary frequencies of the unstable modes are represented as negative values. The fraction of Ni vs Ti displacement in the eigenvectors is shown.[23] The values of the phonon frequencies at the symmetry points are also listed in Table II. Comparison with frequencies at M and R computed with GGA at the corresponding equilibrium lattice parameter of 5.713 a.u. show agreement to within 7 cm^{-1}. All of the eigenvectors at the symmetry points Γ, X, M, and R are uniquely determined by symmetry considerations except for the $M_{5'}$ modes, to be discussed in more detail below. As can be seen from Fig. 1, $X_{1'}$, $X_{5'}$, $M_{1'}$,

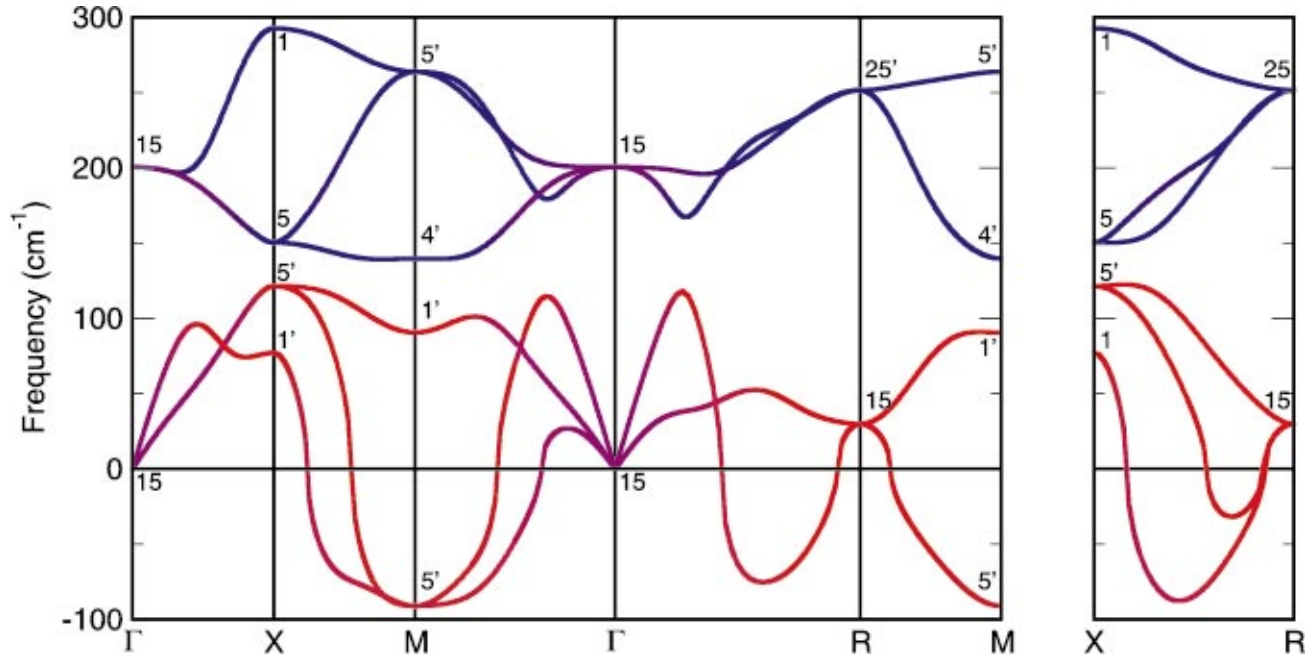

FIG. 1. (Color) Phonon dispersion for NiTi in the $B2$ structure with $a_0=5.594$ a.u. along symmetry lines in the simple cubic BZ. Symmetry labels are assigned according to the conventions of Ref. 24 with Ni at the origin. The imaginary frequencies of the unstable modes are plotted as negative values. The relative importance of Ni relative to Ti displacements is shown by a red-blue colorcode (Ref. 23).

TABLE II. Computed phonon frequencies of $B2$ NiTi with $a_0 = 5.594$ a.u. at the symmetry points in the simple cubic BZ.

Label	Frequency (cm^{-1})	Label	Frequency (cm^{-1})
Γ_{15}	0	R_{15}	30
Γ_{15}	200	R_{25}	252
$X_{1'}$	77	$M_{5'}$	91*i*
$X_{5'}$	121	$M_{1'}$	91
X_5	150	$M_{4'}$	140
X_1	293	$M_{5'}$	264

and R_{15} are pure Ni displacements (red), X_1, X_5, $M_{4'}$, and $R_{25'}$ are pure Ti displacements (blue), and the two Γ_{15} modes are mixed in nearly equal proportions (purple).

As expected on the basis of experimental observation of the low-temperature structure, the $B2$ structure is unstable at $T=0$. The dominant instability is a doubly degenerate $M_{5'}$ mode, with a corresponding two-dimensional space of eigenvectors. The eigenvectors in this space establish directions and magnitude ratios of atomic displacements relative to the $B2$ structure that most effectively lower the structural energy, with all eigenvectors in the space being equally effective at quadratic order in the overall amplitude. Higher order terms are needed to single out the eigenvector(s) that leads to the global minimum. In this case, including terms up to fourth order would yield the two high-symmetry displacement patterns shown in Fig. 2 as the only candidates for the energy minimum. Both resulting structures are orthorhombic and have point groups of the same order. The choice between these two is determined by the actual values of the expansion coefficients, including the effects of strain coupling, which cannot be obtained from the DFPT calculations reported here and will be the subject of a future publication. For the present, we note that the distorted structure produced by freezing the eigenvector in Fig. 2(a) into the reference cubic structure yields, with an appropriate choice of overall amplitude, an excellent approximation to the observed ground-state $B19'$ structure. This is nontrivial, since the ratios of the

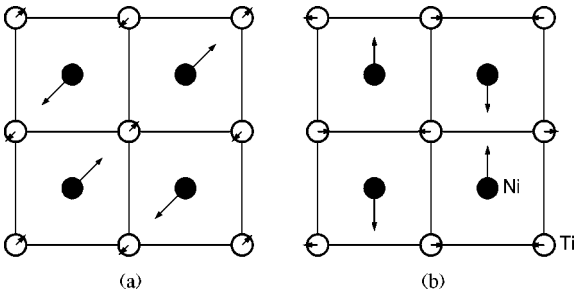

FIG. 2. Atomic displacement patterns corresponding to two linearly independent eigenvectors of the unstable M_5' mode at $\vec{k} = (2\pi/a_0)(\frac{1}{2}\frac{1}{2}0)$, transforming as (a) $\hat{x}+\hat{y}$ and (b) $\hat{y}$. Here, a portion of the $B2$ structure, with Ni atoms shown by filled circles and Ti atoms shown by open circles, is viewed along the (001) direction. All displacements lie in the x-y plane. The ratio of arrow lengths is equal to the ratio of Ni to Ti displacements in the computed eigenvector. Both resulting structures are orthorombic.

TABLE III. Structural parameters of $B2$ NiTi distorted by "freezing in" the eigenvector in Fig. 2(a), $a=2.960$ Å, $b=4.186$ Å, $c=4.186$ Å, $\gamma=90°$, compared with the experimental monoclinic $B19'$ structure (Ref. 25), $a=2.898$ Å, $b=4.646$ Å. $c=4.108$ Å, $\gamma=97.78°$. While the distorted $B2$ structure actually has space group $Pmma$, the structure is presented within $P2_1/m$, the space group of the $B19'$ structure, to facilitate comparison.

Structure	Wyckoff position	x	y	z
distorted $B2$	Ti(2e)	0.5	0.235	0.25
	Ni(2e)	0	0.708	0.25
$B19'$	Ti(2e)	0.4176	0.2164	0.25
	Ni(2e)	0.0372	0.6752	0.25

Ni and Ti displacements in the two $M_{5'}$ modes (the other at high frequency) are not determined by symmetry, but can be obtained only by computing and diagonalizing the dynamical matrix. As can be seen in Table III, the main difference is in the angle γ, lowering the symmetry from orthorhombic to monoclinic.

While the evolution of the lattice instability away from the zone center cannot be directly obtained experimentally, Fig. 1 shows that the unstable phonon branches actually extend throughout the Brillouin zone. From the M point, the instability extends more than half of the way to Γ and X. At Γ, the acoustic branches behave normally at very small $\vec{q}$. As $\vec{q}$ increases along Γ-R and Γ-M, one and two individual optic modes, respectively, disperse strongly downward, mixing with the acoustic branches and then becoming unstable. As the R point is approached along Γ-R, the unstable longitudinal mode turns around and becomes stable once again. Along Γ-X the Δ_1 optic mode similarly disperses downward and mixes with the Δ_1 acoustic branch, although along this line all phonon modes remain stable.

The origin of the lattice instability in NiTi can be explored through analysis of the interatomic force constants (IFC's) in real space. The important features of the phonon dispersion in Figure 1 are well reproduced by a simple force constant model in which most of the IFC's are set to zero and only a few of the largest IFC's are retained. These are given in Table IV. The importance of noncentral forces is illustrated by the fact that $C_{xx}(0,\mathrm{Ni};0,\mathrm{Ti})$ is nonzero. Indeed, it is of the same magnitude as $C_{xy}(0,\mathrm{Ni};0,\mathrm{Ti})$. Furthermore, as

TABLE IV. Selected interatomic force constants $C_{\alpha\beta}(0,\kappa;l',\kappa')$(Ry/Bohr^2) of $B2$ NiTi. The values in brackets are set to zero in the simple force constant model discussed in the text. The index l' indicates the unit cell centered at $l'a_0\hat{x}$.

Atoms	α,β	$l'=0$	$l'=1$	$l'=2$	$l'=3$
Ni-Ni	xx	0.0321	0.0161	($\approx$0)	−0.0032
	yy	0.0321	0.003	($\approx$0)	($\approx$0)
Ti-Ti	xx	0.1431	−0.043	0.0082	($\approx$0)
	yy	0.1431	0.0049	($\approx$0)	($\approx$0)
Ni-Ti	xx	−0.0078	−0.0025	($\approx$0)	($\approx$0)
	xy	−0.0120	($\approx$0)	($\approx$0)	($\approx$0)

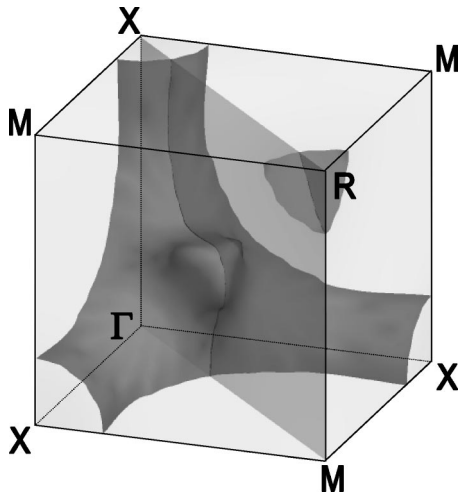

FIG. 3. Zero-frequency isosurfaces of the phonon dispersion relation in the first octant of the Brillouin zone. Outside the interpenetrating tubes along the (001) directions and the small spheres centered at *R*, at least one phonon mode is unstable.

suggested by the large Ni displacements in Fig. 2 and confirmed by the relative Ni vs Ti character of individual phonon branches in Fig. 1, the instabilities throughout the zone are dominated by the energetics of Ni displacements. In fact, if the Ti sublattice is frozen in the positions corresponding to the $B2$ structure, the resulting pure-Ni modes display the characteristic downward-dispersing behavior of the optic modes described above, including the resulting instability at M and the upturn along Γ-R.

The $\vec{q}$ dependence of the unstable modes can be more easily visualized in a three-dimensional view of the BZ showing the $\omega^2=0$ isosurface (Fig. 3). The region of stability is confined to three interpenetrating tubes along the Cartesian axes, with additional bulges in the central region along the Γ-R directions, and to small approximately spherical regions around the R points. The unstable modes at M are thus continuously connected to the unstable mode along Γ-R. The fact that the unstable mode extends through such a large fraction of the Brillouin zone directly implies that the minimal unstable localized displacement pattern is very tightly localized. In fact, as can be explicitly verified using the IFC's in Table IV, the $B2$ structure is unstable against the displacement of a single Ni coordinated with much smaller displacements of the surrounding eight Ti atoms.

Frequencies of acoustic phonons along symmetry lines in the high-temperature $B2$ phase have been experimentally measured.[26] Comparison with the results of our calculations shows that while the calculated stable acoustic mode frequencies at R, X, and M are in general agreement with their experimental counterparts, the unstable branches are dramatically renormalized by temperature effects. Through decomposition of the force constants into a short-range part and a long-range electronic part, the semiempirical analysis of Ref. 27 showed that temperature dependence due to Fermi surface smearing is significant only near the wave vector associated with the transition to the intermediate temperature R phase. This leads us to speculate that the temperature stabilization in most of the Brillouin zone results from anharmonic phonon-phonon interactions. Indeed, the high-temperature $B2$ structure is entropically stabilized and should be characterized by large local fluctuations away from the high-symmetry average positions of the atoms. As in the previous work on $KNbO_3$,[2] the nature of these distortions is directly related to the minimal unstable localized displacement pattern, and could be experimentally investigated through diffuse x-ray scattering or with local probes, such as EXAFS. The extension of our work to theoretical investigation of the phase diagram and temperature dependence of the phonon dispersion requires a first-principles effective Hamiltonian analysis, analogous to that for the perovskite oxides, but beyond the scope of the present paper.

IV. CONCLUSIONS

In conclusion, we performed *ab initio* calculations of the phonon dispersion of the $B2$ high-symmetry reference structure of NiTi. There are lattice instabilities throughout the entire Brillouin zone, with the dominant instability at M. An excellent approximation to the observed ground state structure of NiTi can be generated by freezing in a particular choice of eigenvector from the corresponding two-dimensional space with adjustment of the overall amplitude.

ACKNOWLEDGMENTS

We thank R. D. James, K. Bhattacharya, and I. I. Naumov for valuable discussions. This work was supported by AFOSR/MURI F49620-98-1-0433. A portion of the calculations were performed on the SGI Origin 2000 at ARL MSRC.

[1] R. D. King-Smith and D. Vanderbilt, Phys. Rev. B **49**, 5828 (1994).
[2] R. Yu and H. Krakauer, Phys. Rev. Lett. **74**, 4067 (1995).
[3] Ph. Ghosez, E. Cockayne, U. V. Waghmare, and K. M. Rabe, Phys. Rev. B **60**, 836 (1999).
[4] U. V. Waghmare and K. M. Rabe, Phys. Rev. B **55**, 6161 (1997).
[5] R. D. James and K. F. Hane, Acta Mater. **48**, 197 (2000).
[6] R. F. Hehemann and G. D. Sandrock, Scr. Metall. **5**, 801 (1971).
[7] Y. Y. Ye, C. T. Chan, and K. M. Ho, Phys. Rev. B **56**, 3678 (1997).
[8] M. Sanati, R. C. Albers, and F. J. Pinski, Phys. Rev. B **58**, 13 590 (1998).
[9] M. E. Lines and A. M. Glass, *Principles and Applications of Ferroelectrics and Related Materials* (Clarendon, Oxford, 1977).
[10] N. E. Zein, Sov. Phys. Solid State **26**, 1825 (1984); S. Baroni, P. Giannozzi, and A. Testa, Phys. Rev. Lett. **58**, 1861 (1987).
[11] S. Baroni, S. de. Gironcoli, A. Dal Corso, and P. Giannozzi, http://www.sissa.it/cm/PWcodes
[12] J. P. Perdew and A. Zunger, Phys. Rev. B **23**, 5048 (1981).

[13] J. P. Perdew, K. Burke, and M. Ernzerhof, Phys. Rev. Lett. **77**, 3865 (1996).
[14] D. Vanderbilt, Phys. Rev. B **41**, 7892 (1990).
[15] A. M. Rappe, K. M. Rabe, E. Kaxiras, and J. D. Joannopoulos, Phys. Rev. B **41**, 1227 (1990).
[16] A. DalCorso, A. Pasquarello, and A. Baldereschi, Phys. Rev. B **56**, 11 369 (1997).
[17] M. Methfessel and A. T. Paxton, Phys. Rev. B **40**, 3616 (1989).
[18] P. Giannozzi, S. de Gironcoli, P. Pavone, and S. Baroni, Phys. Rev. B **43**, 7231 (1991).
[19] P. Blaha, K. Schwarz, and J. Luitz, WIEN97, Vienna University of Technology, Vienna 1997. [Improved and updated Unix version of the original copyrighted WIEN code, published by P. Blaha, K. Schwarz, P. Sorantin, and S. B. Trickey, in Comput. Phys. Commun. **59**, 399 (1990).] Our FLAPW calculations were performed using a 56 *k*-point mesh in the $\frac{1}{48}$ irreducible wedge. No shape approximations were made to the density or potential. A $R_{\mathrm{MT}}K_{\mathrm{max}}$ of 11 were used. The Gaussian smearing method with a width of 0.001 Ry was used in the Brillouin zone integrations.
[20] E. Goo and R. Sinclar, Acta Metall. **33**, 1717 (1985); K. Otsvka, T. Sawamura, and K. Shimizu, Phys. Status Solidi A **5**, 457 (1971).
[21] O. Mercier, K. N. Melton, G. Gremand, and J. Hägi, J. Appl. Phys. **51**, 1833 (1980).
[22] F. Birch, J. Geophys. Res. **83**, 1257 (1978).
[23] A color has been assigned to each eigenvalue, determined by the fraction of Ni and Ti squared displacements in the normalized eigenvector of the dynamical matrix (red for the Ni atom and blue for the Ti atom).
[24] F. Bassani and G. Pastori Parravicini, *Electronic States and Optical Transitions in Solids*, edited by R. A. Ballinger (Pergamon, Oxford, 1975).
[25] Y. Kudoh, M. Tokonami, S. Miyazaki, and K. Otsuka, Acta Metall. Mater. **33**, 2049 (1985).
[26] H. Tietz, M. Müllner, and B. Renker, J. Phys. C **17**, L529 (1984).
[27] G. L. Zhao and B. N. Harmon, Phys. Rev. B **48**, 2031 (1993).